Supporting Information
For

Terminal {Ni(II)-SH} Complex Promoted Anaerobic Catalytic Sulfur Atom Transfer Reaction: Implication to sulfide oxidase function of Cu/Zn-Superoxide Dismutase

Jayanta Bag, Surajit Das and Kuntal Pal*

Department of Chemistry, University of Calcutta, 92 APC Road, Kolkata 700 009, India

Contents

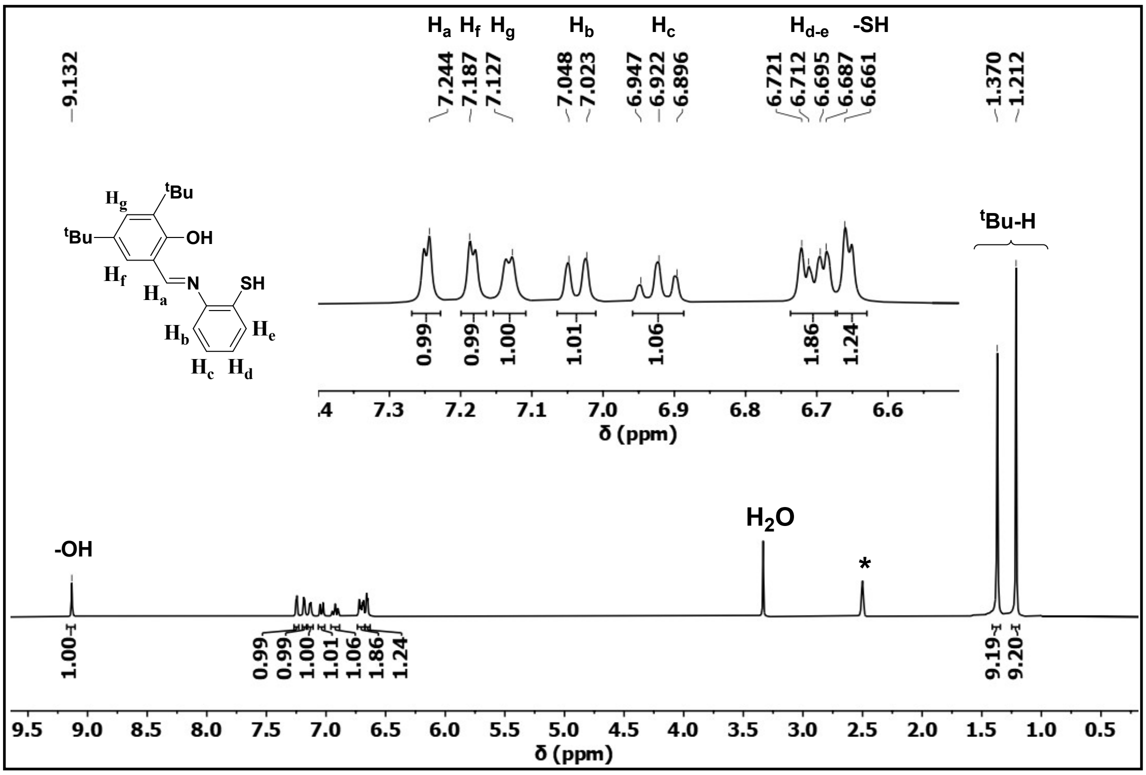

Figure S1: ^{1}H NMR spectrum (400 MHz, DMSO-d$_6$) of **H$_2$L^{tBu}**

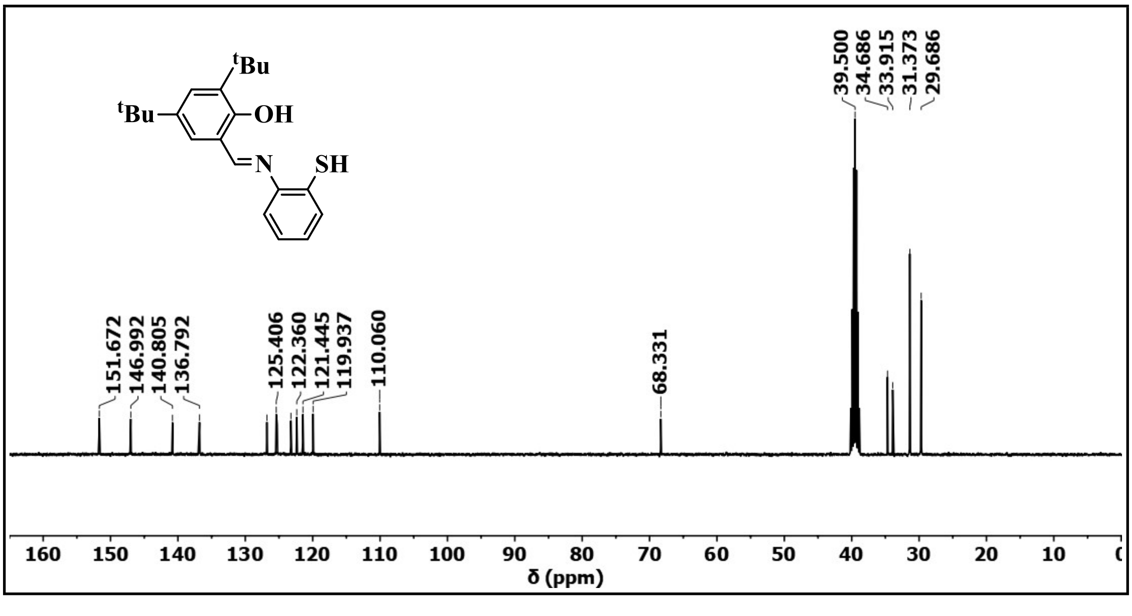

Figure S2: ^{13}C NMR spectrum (400 MHz, DMSO-d$_6$) of **H$_2$L^{tBu}**

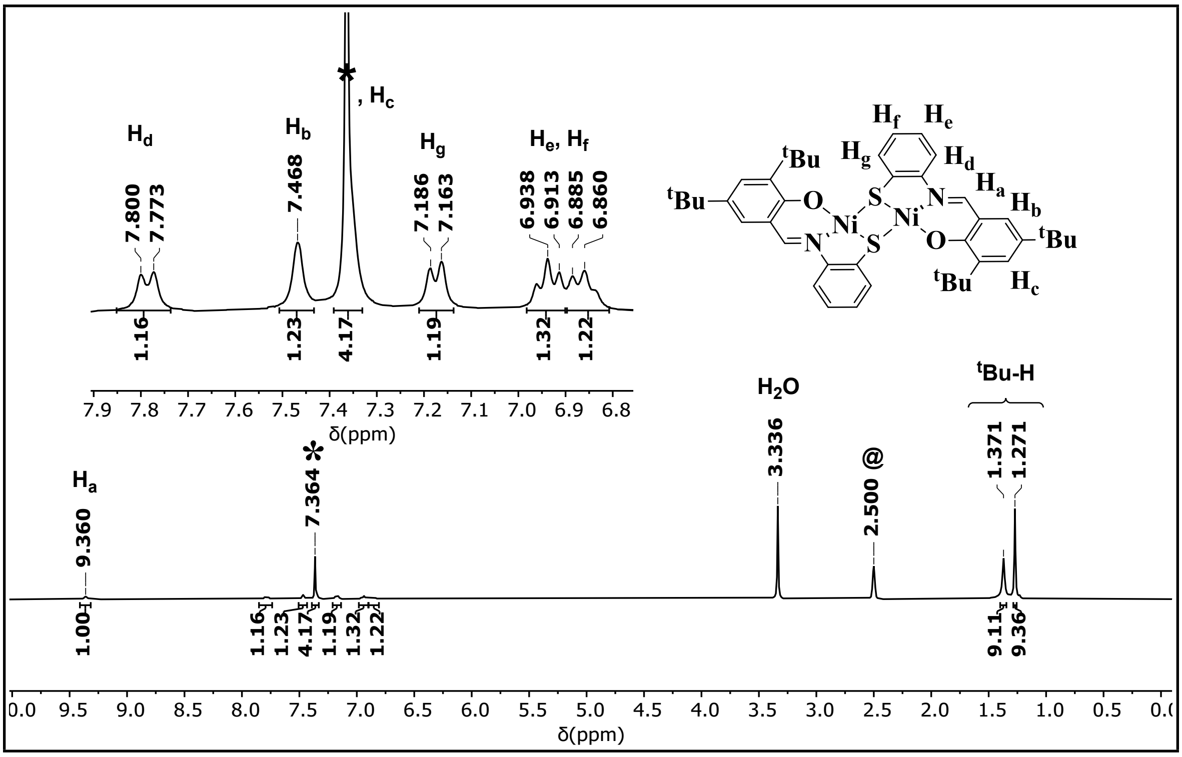

Figure S3A: ^{1}H NMR spectrum (400 MHz, DMSO-d$_6$) of [(NiL^{tBu})$_2$] **(1^{tBu})**

*Benzene, @ DMSO-d$_6$

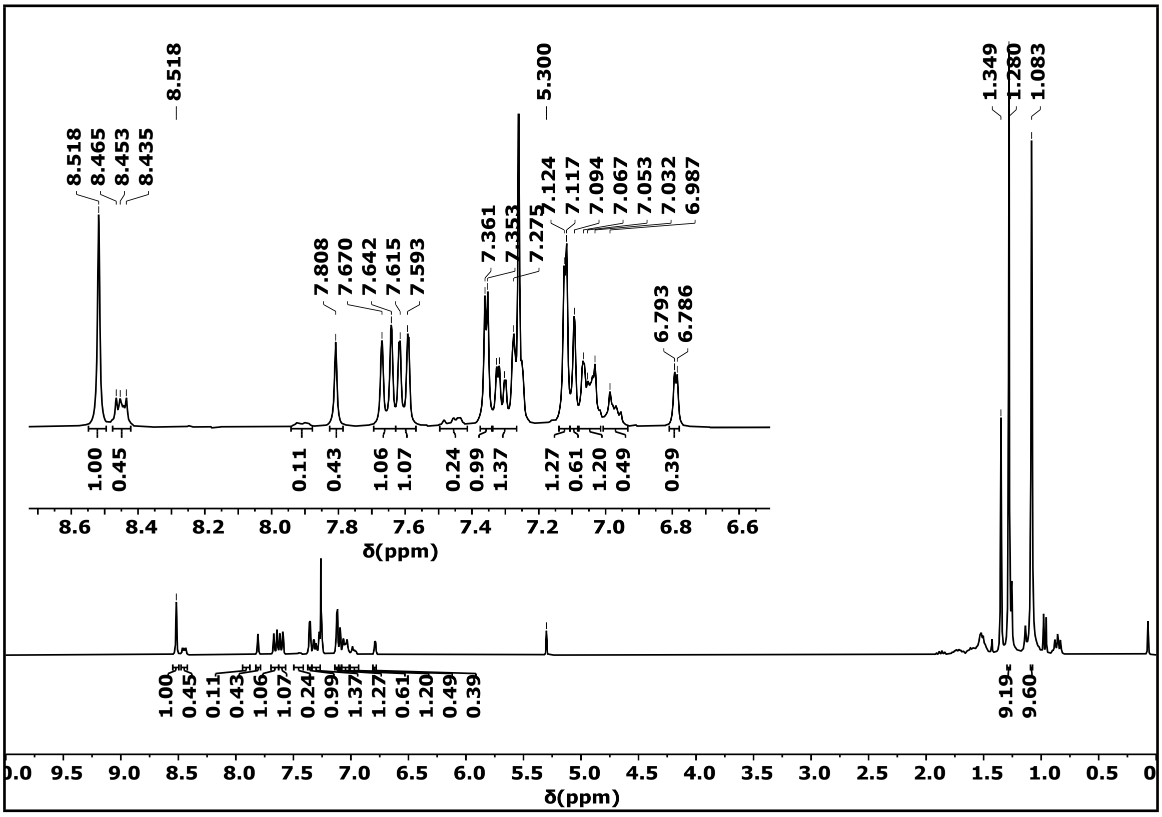

Figure S3B: ^{1}H NMR spectrum (400 MHz, CDCl$_3$) of **1^{tBu}**

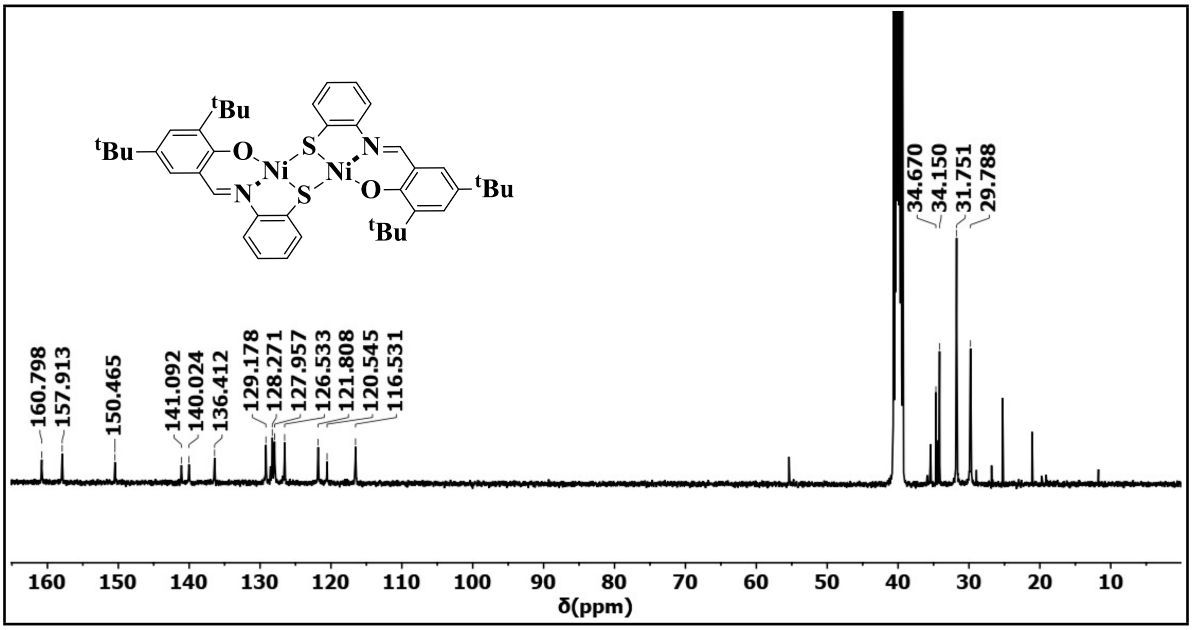

Figure S4: ^{13}C NMR spectrum (400 MHz, DMSO-d$_6$) of [(NiL^{tBu})$_2$] (1^{tBu})

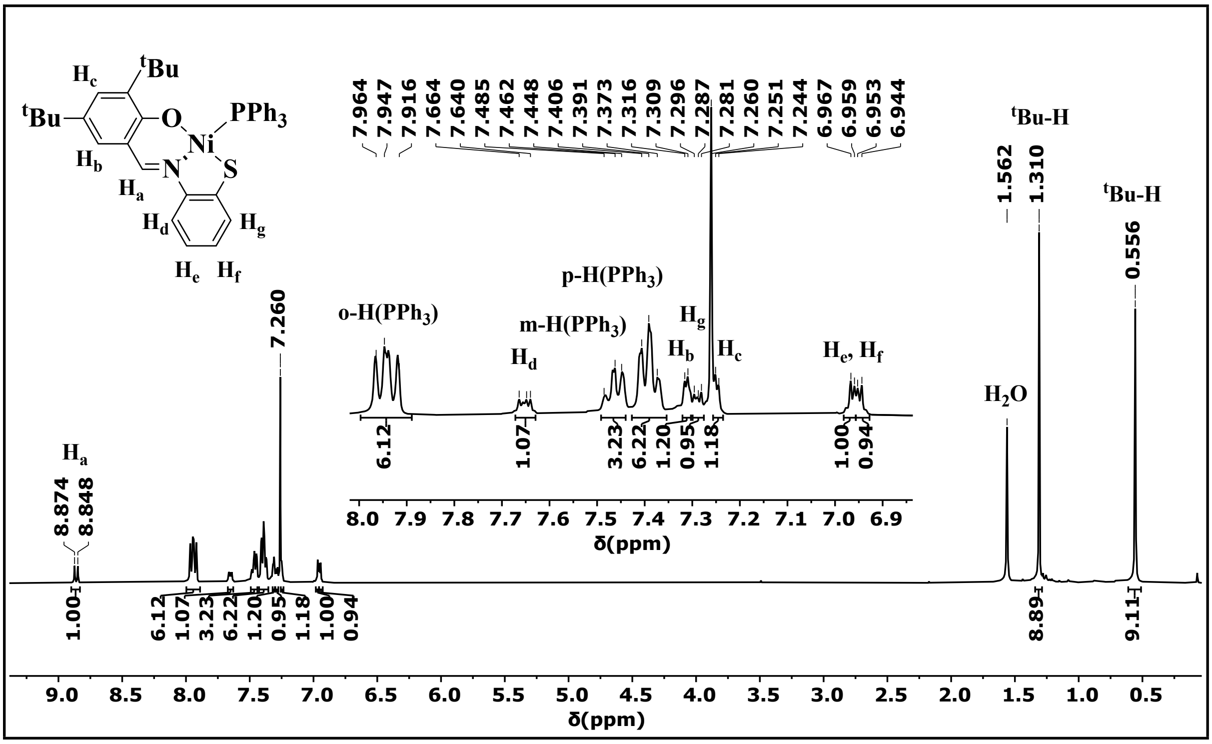

Figure S5: ^{1}H NMR spectrum (400 MHz, CDCl$_3$) of [NiL^{tBu}(PPh$_3$)] (**2^{tBu}**)

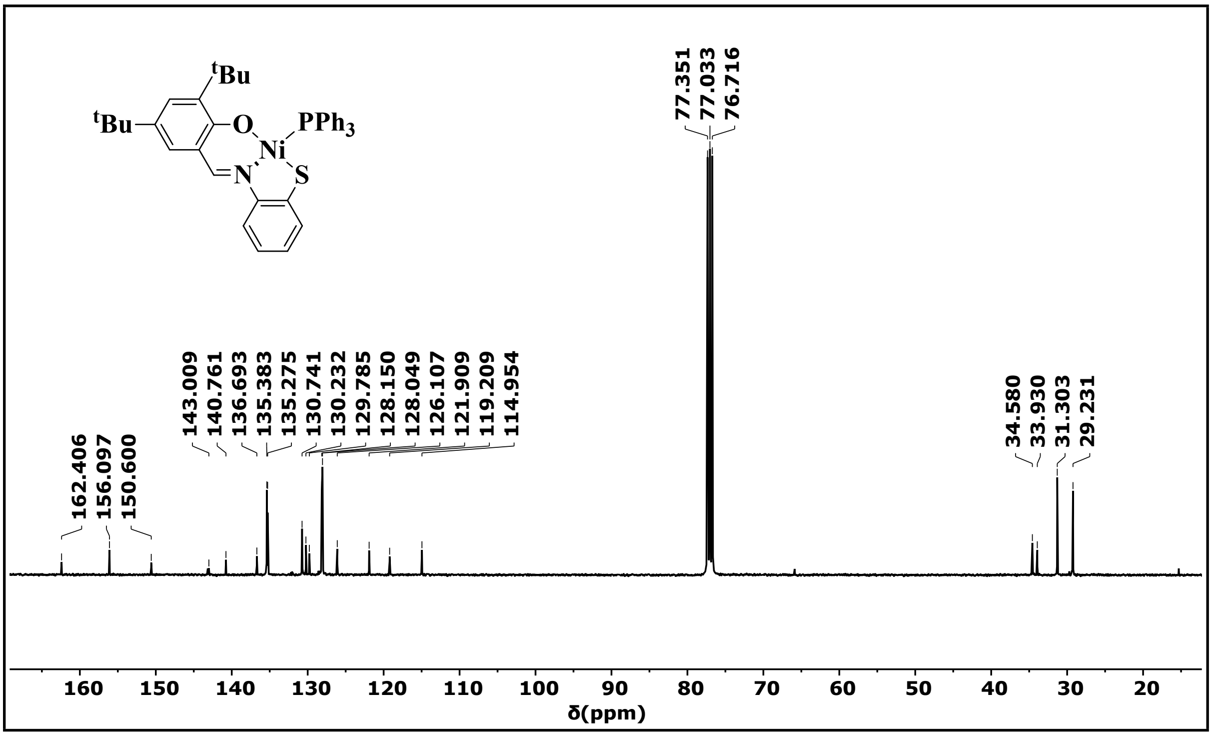

Figure S6: ^{13}C NMR spectrum (400 MHz, $CDCl_3$) of [$NiL^{tBu}(PPh_3)$] **(2^{tBu})**

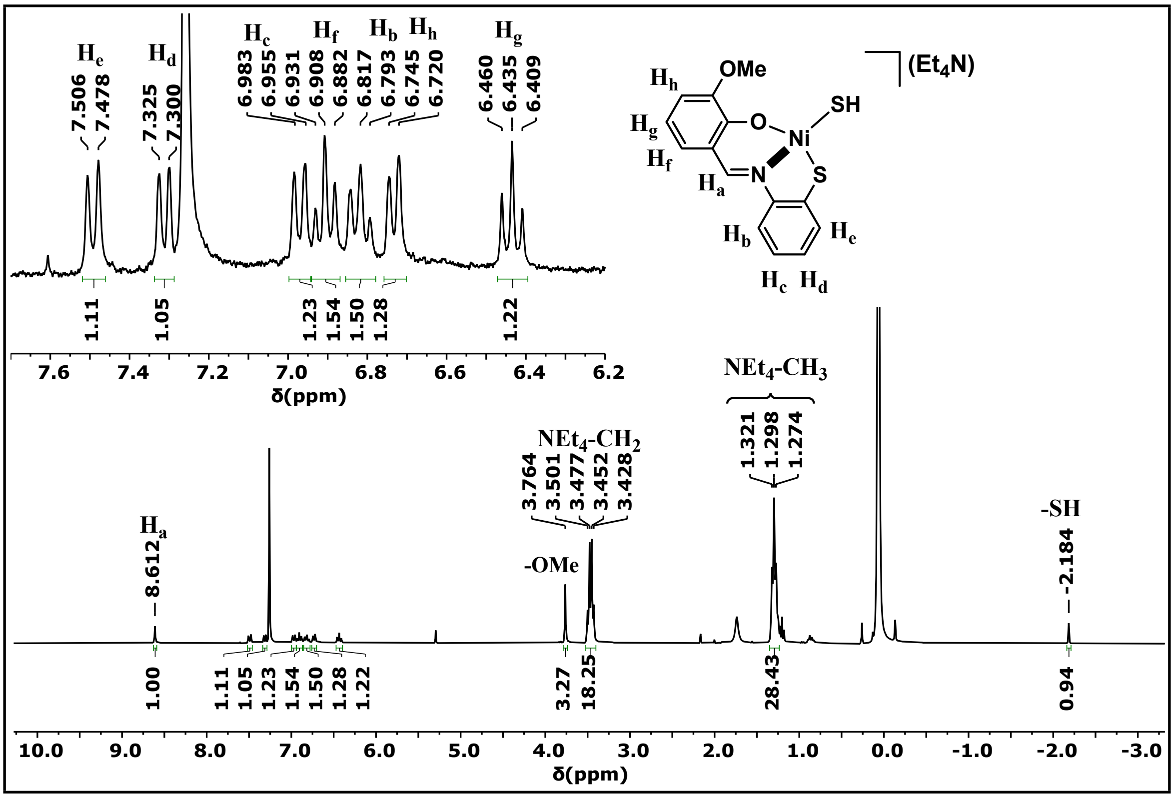

Figure S7: ^{1}H NMR spectrum (400 MHz, $CDCl_3$) of[$NiL^{OMe}(SH)$] **(3^{OMe}. (Et_4N)**)

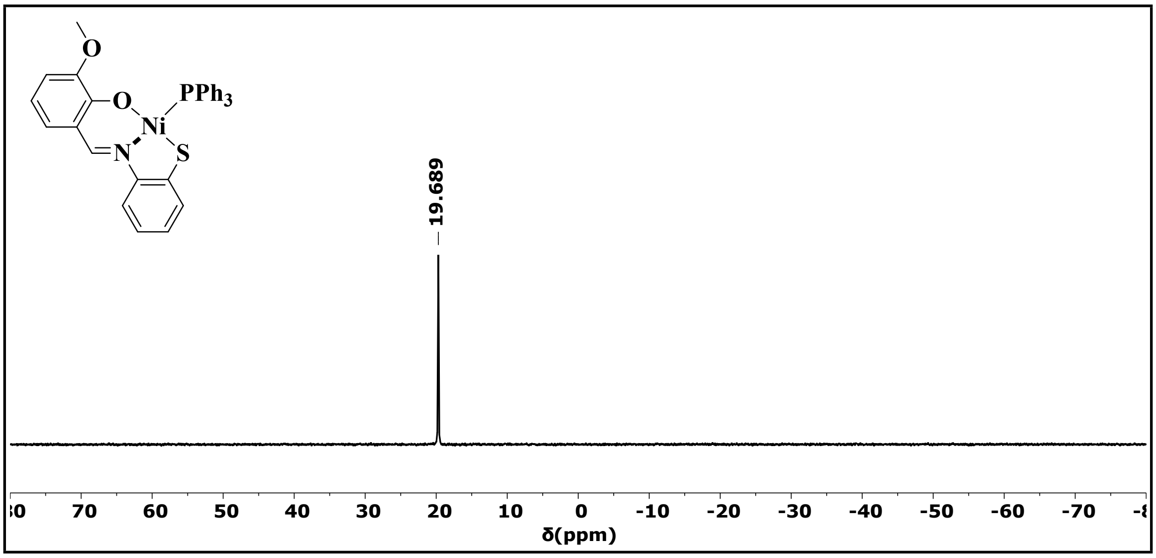

Figure S9: $^{31}P\{^1H\}$ NMR spectrum (400 MHz, $CDCl_3$) of [NiL^{OMe}(PPh_3)] (**3^{OMe}**).

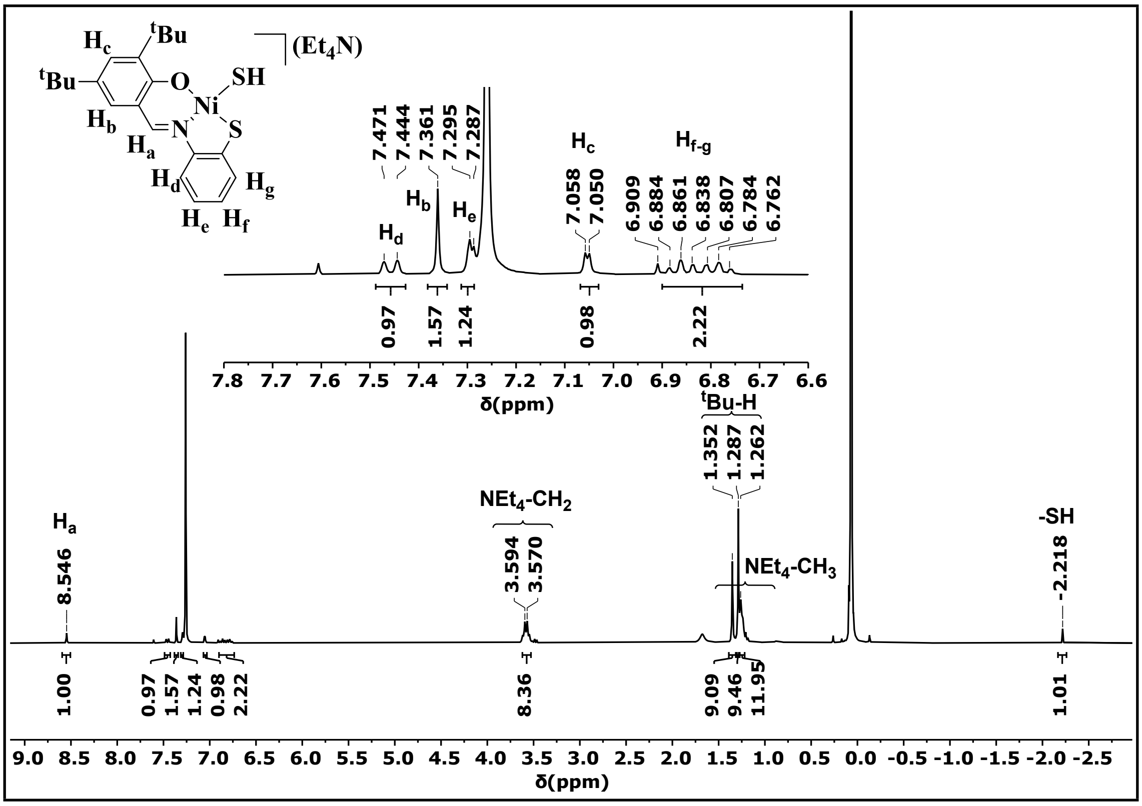

Figure S10: ^1H NMR spectrum (400 MHz, $CDCl_3$) of [NiL^{tBu}(SH)](**3^{tBu}. (Et_4N)**).

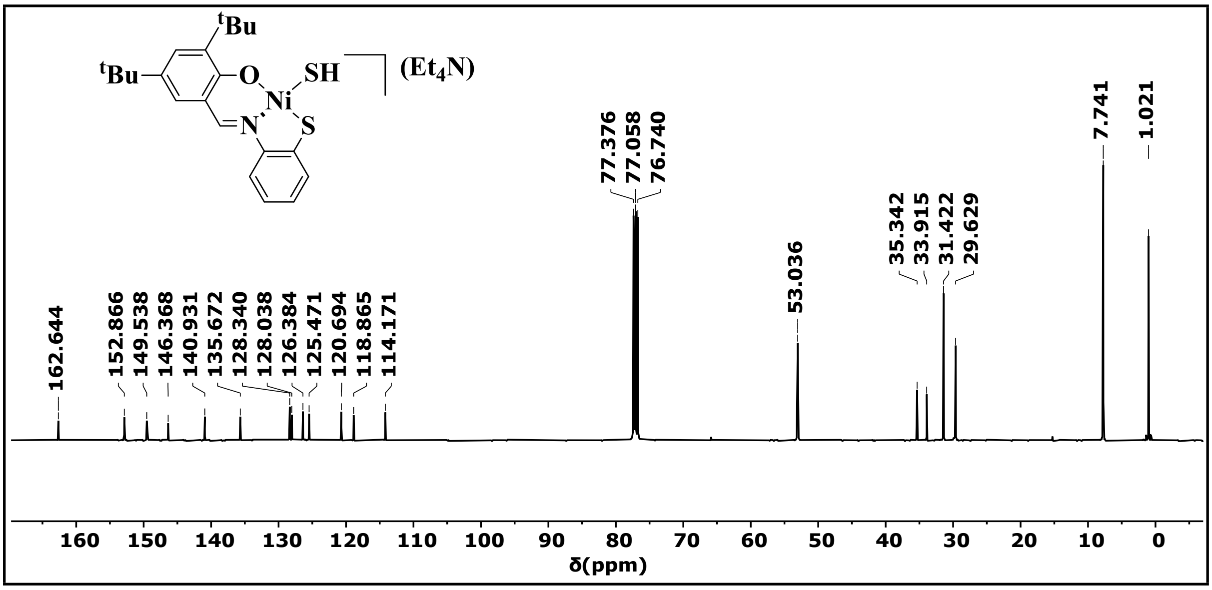

Figure S11: ^{13}C NMR spectrum (400 MHz, $CDCl_3$) of [NiL^{tBu}(SH)](**3^{tBu}. (Et_4N)**)

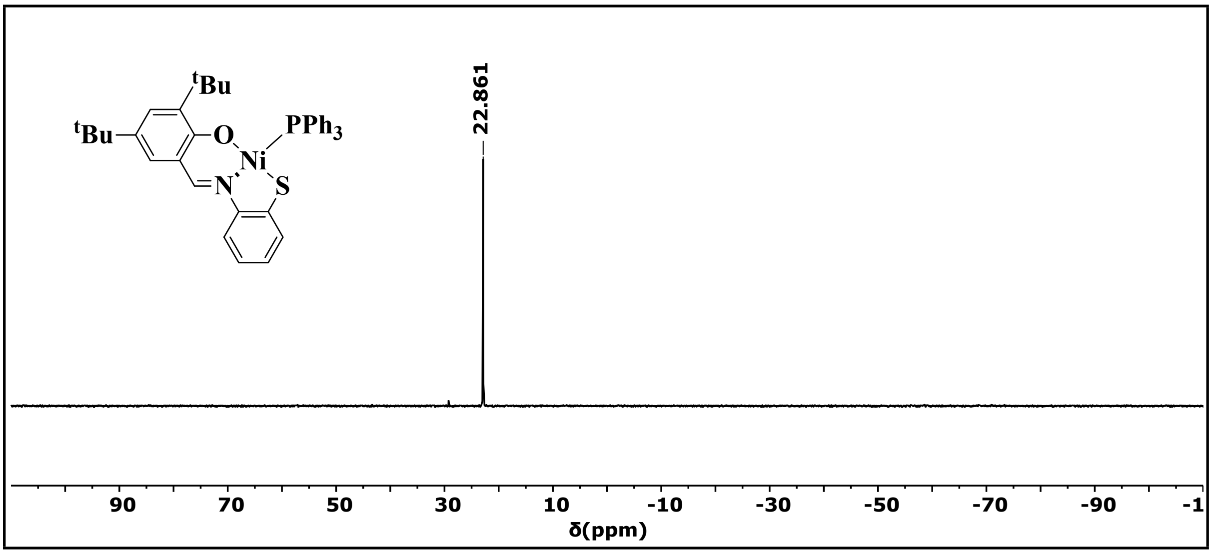

Figure S12: $^{31}P\{^1H\}$ NMR spectrum (400 MHz, $CDCl_3$) of [NiL^{tBu}(PPh_3)] **(2^{tBu})**.

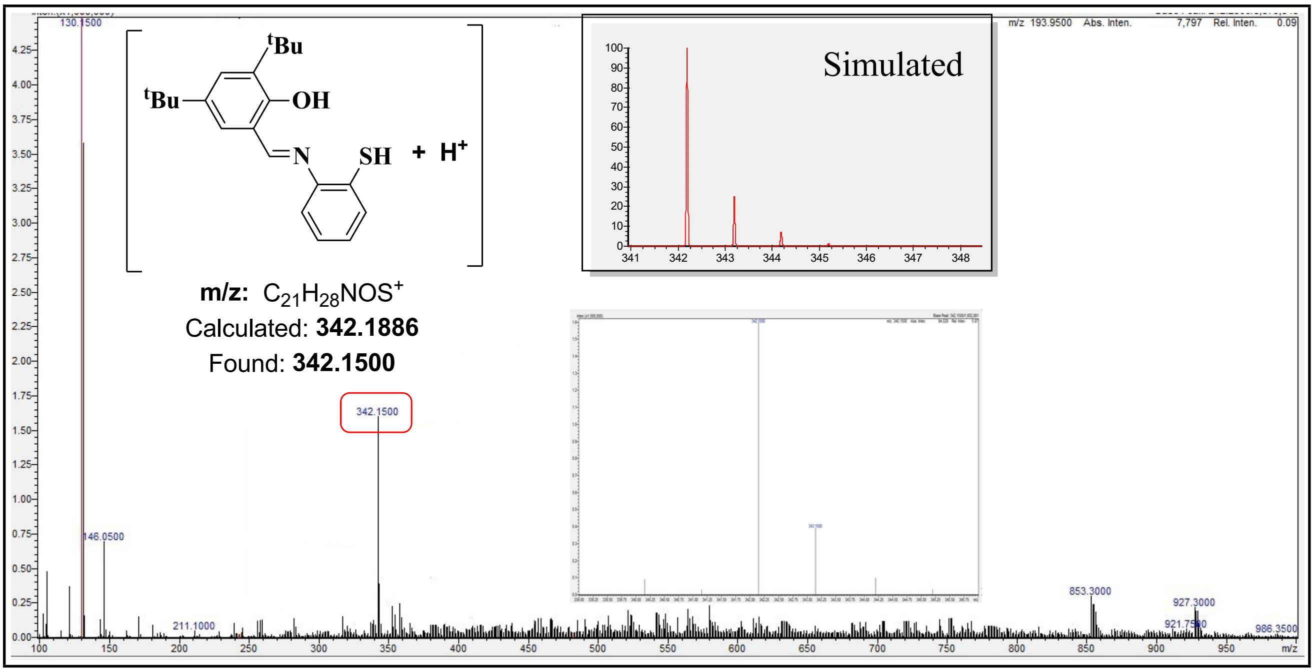

Figure S13: LC-MS mass spectrum of $\mathbf{H_2L^{tBu}}$ along with simulated spectrum inset (using Isopro3.0 program).

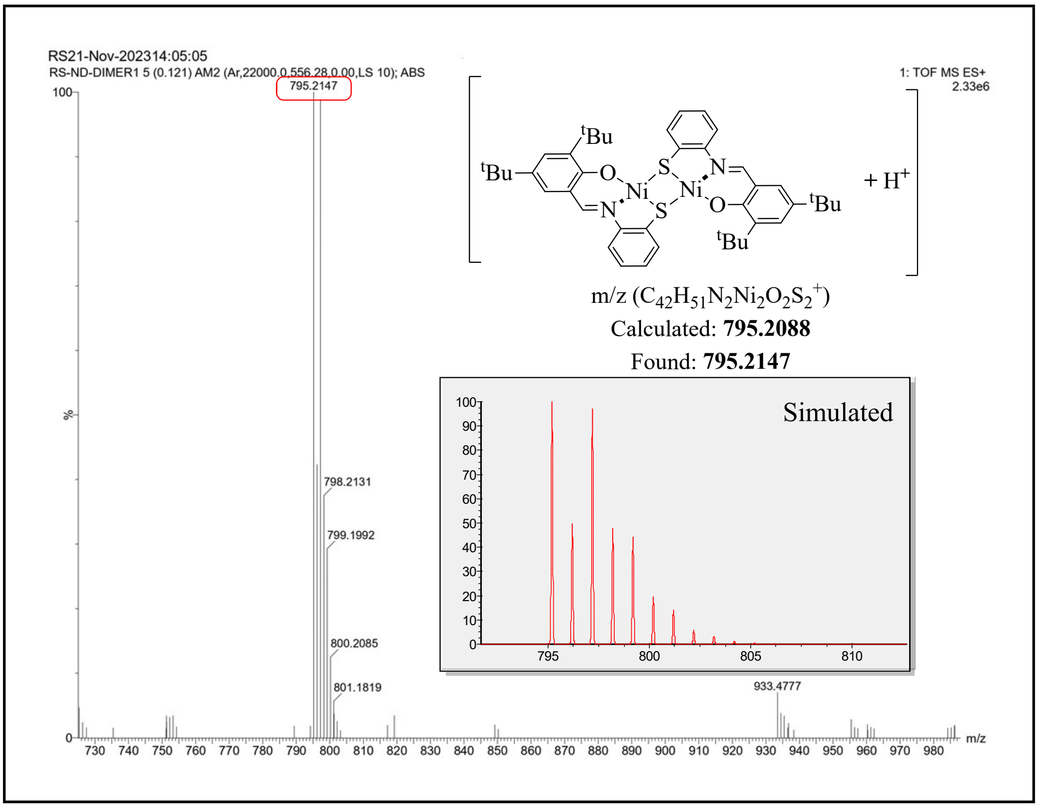

Figure S14: HRMS (ESI$^+$) spectrum of [(NiL^{tBu})$_2$] (1^{tBu}) along with simulated spectrum inset (using Isopro3.0 program).

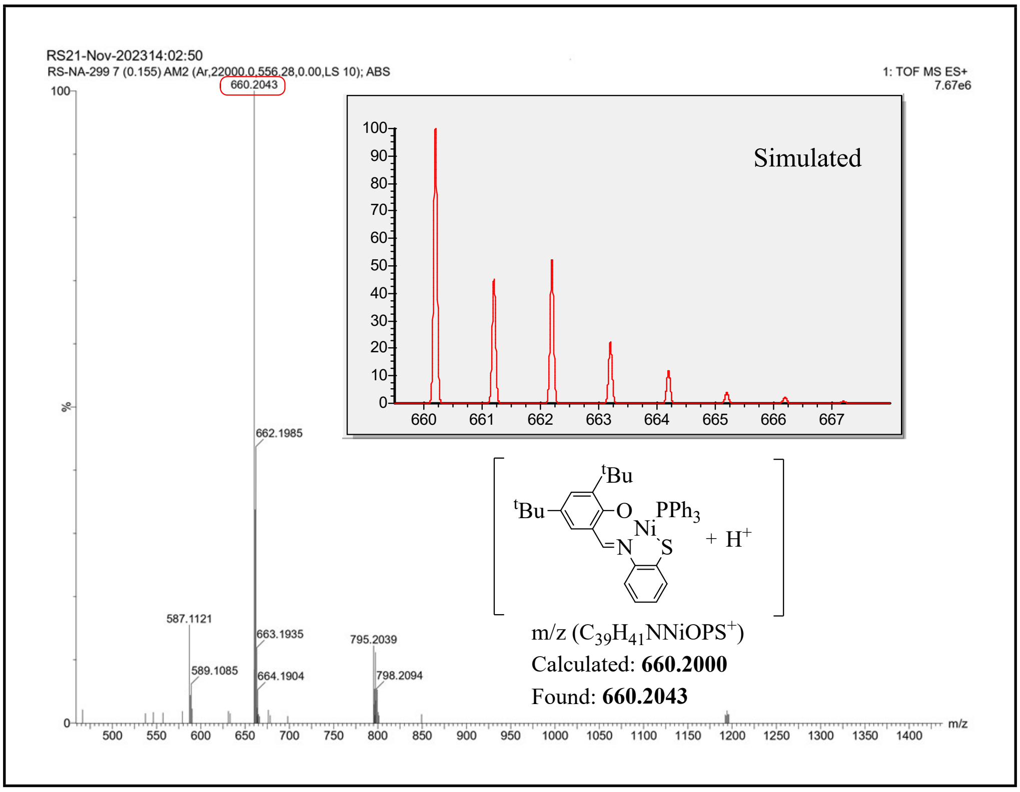

Figure S15: HRMS (ESI^{+}) spectrum of [NiL^{tBu}(PPh$_3$)] (2^{tBu}) along with simulated spectrum inset (using Isopro3.0 program).

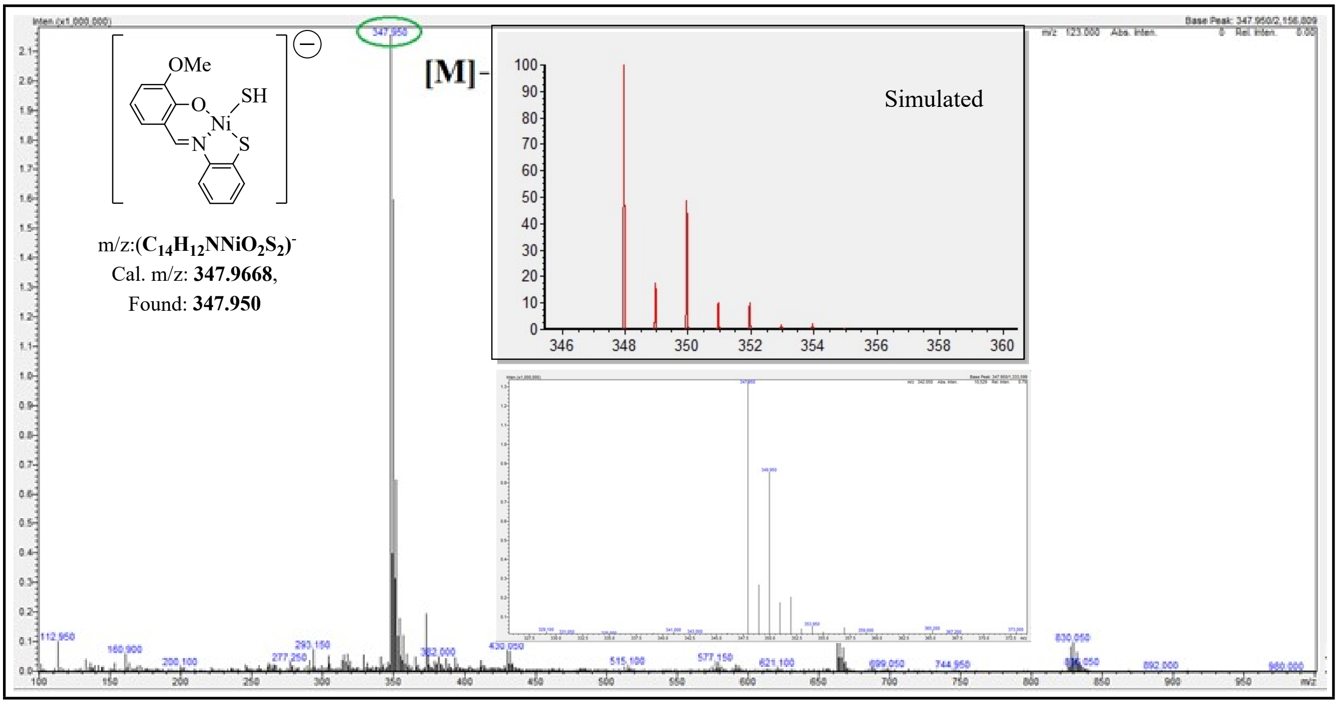

Figure S16: LCMS (ESI$^-$) spectrum of [NiL^{OMe}(SH)] (**3^{OMe}. (Et$_4$N)**) along with simulated spectrum inset (using Isopro3.0 program).

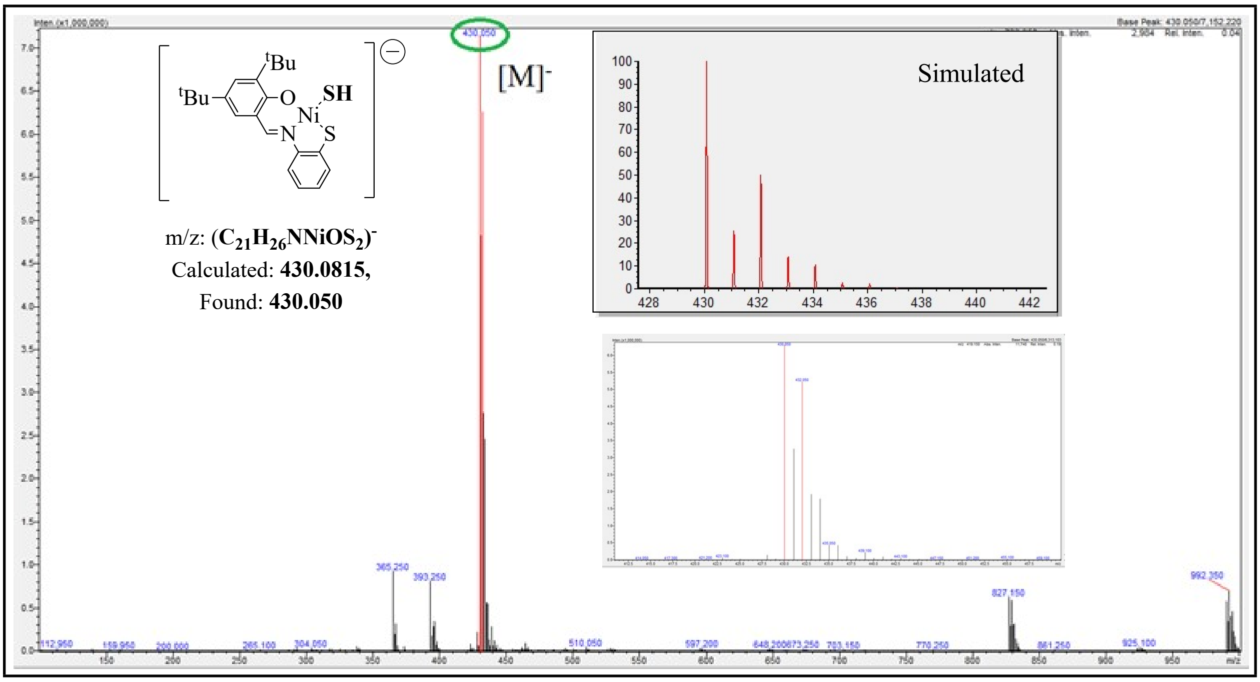

Figure S17: LC-MS (ESI$^-$) spectrum of [NiL^{tBu}(SH)] (**3^{tBu}. (Et$_4$N)**) along with simulated spectrum inset (using Isopro3.0 program).

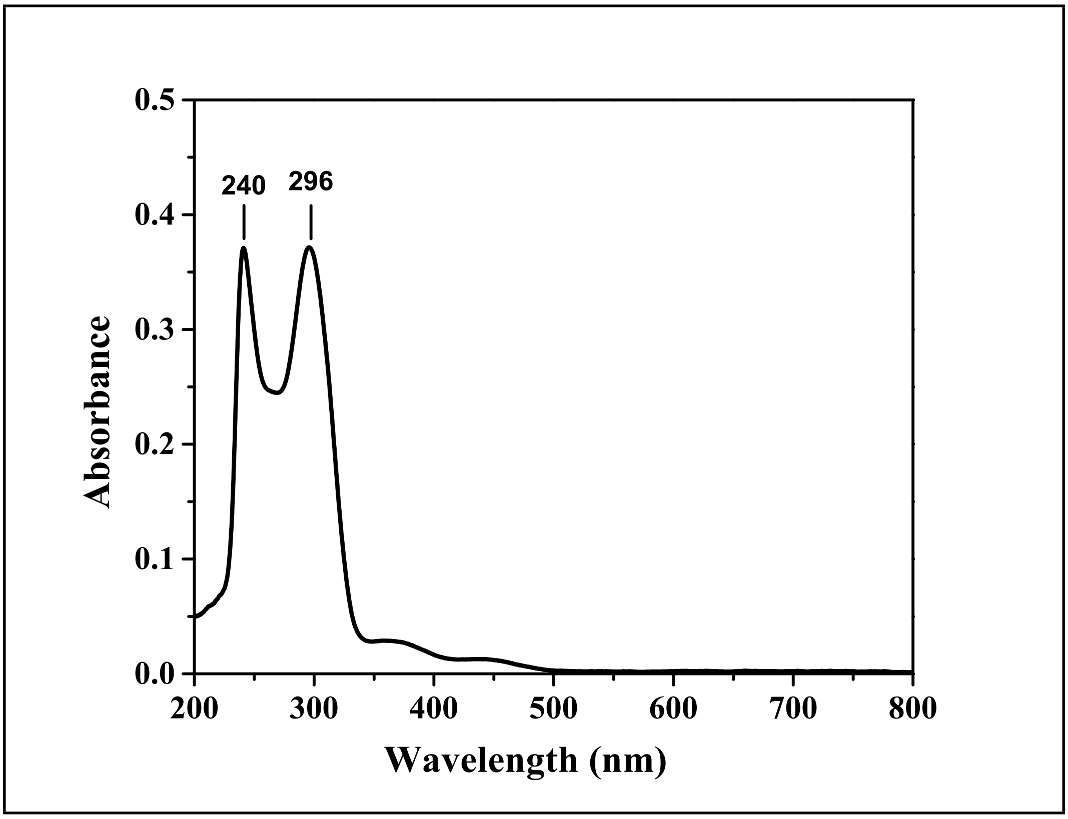

Figure S18: UV-vis spectra of $\mathbf{H_2L^{tBu}}$(5x10^{-5}(M) in acetonitrile at 25 °C).

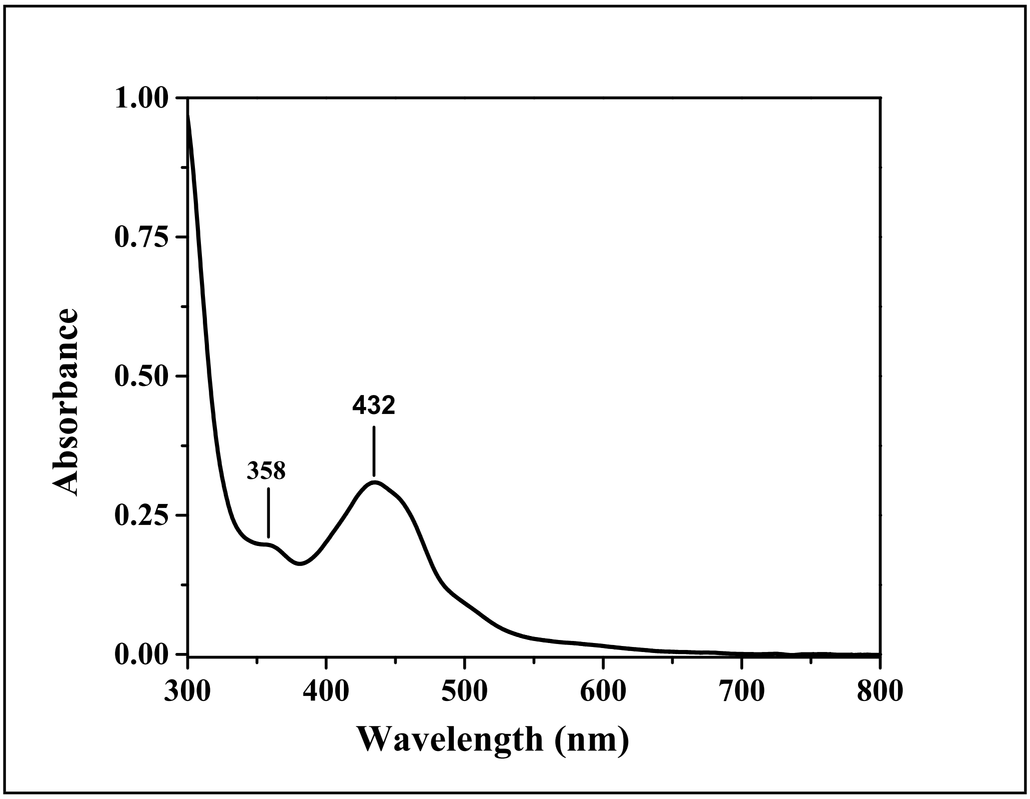

Figure S19: UV-vis spectra of[$(NiL^{tBu})_2$] ($\mathbf{1^{tBu}}$) (5x10^{-5}(M) in acetonitrile at 25 °C)

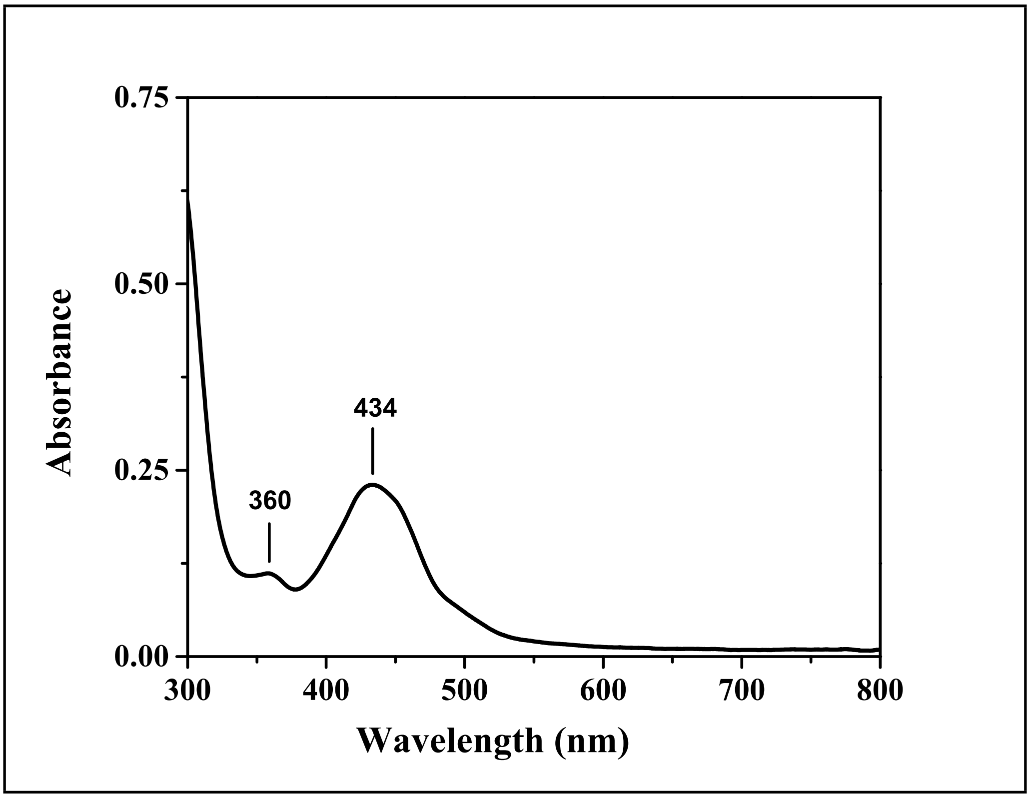

Figure S20: UV-vis spectra of [NiL^{tBu}(PPh$_3$)] **(2^{tBu})** (5x10^{-5}(M) in acetonitrile at 25 °C)

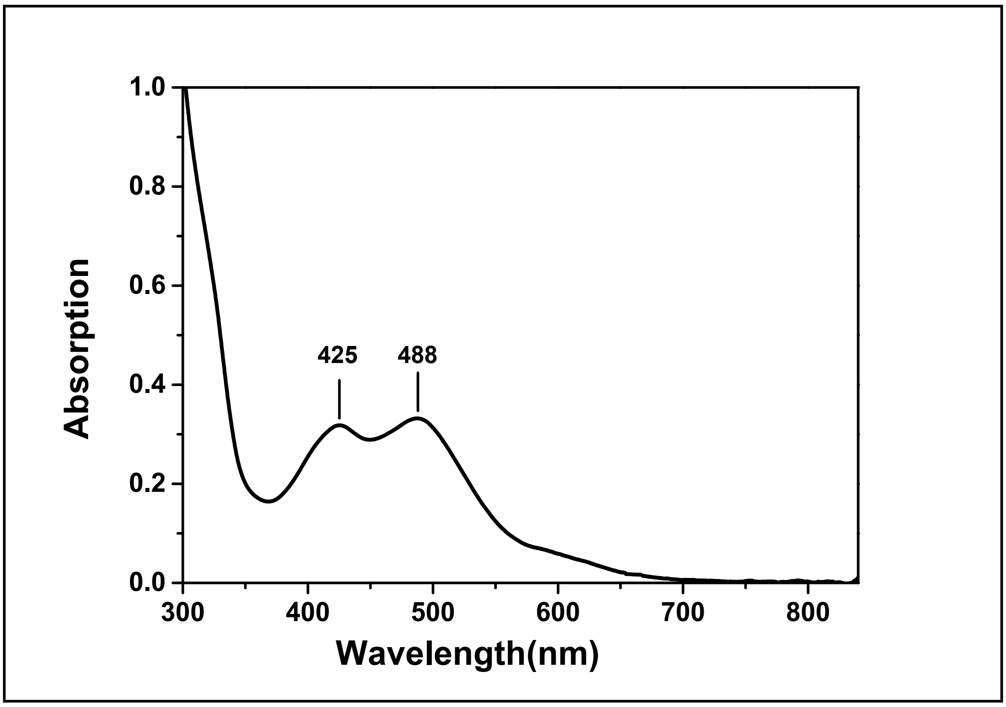

Figure S21: UV-vis spectra of [NiL^{OMe}(SH)] (**3^{OMe}. (Et$_4$N)**) (5x10^{-5}(M) in acetonitrile at 25 °C)

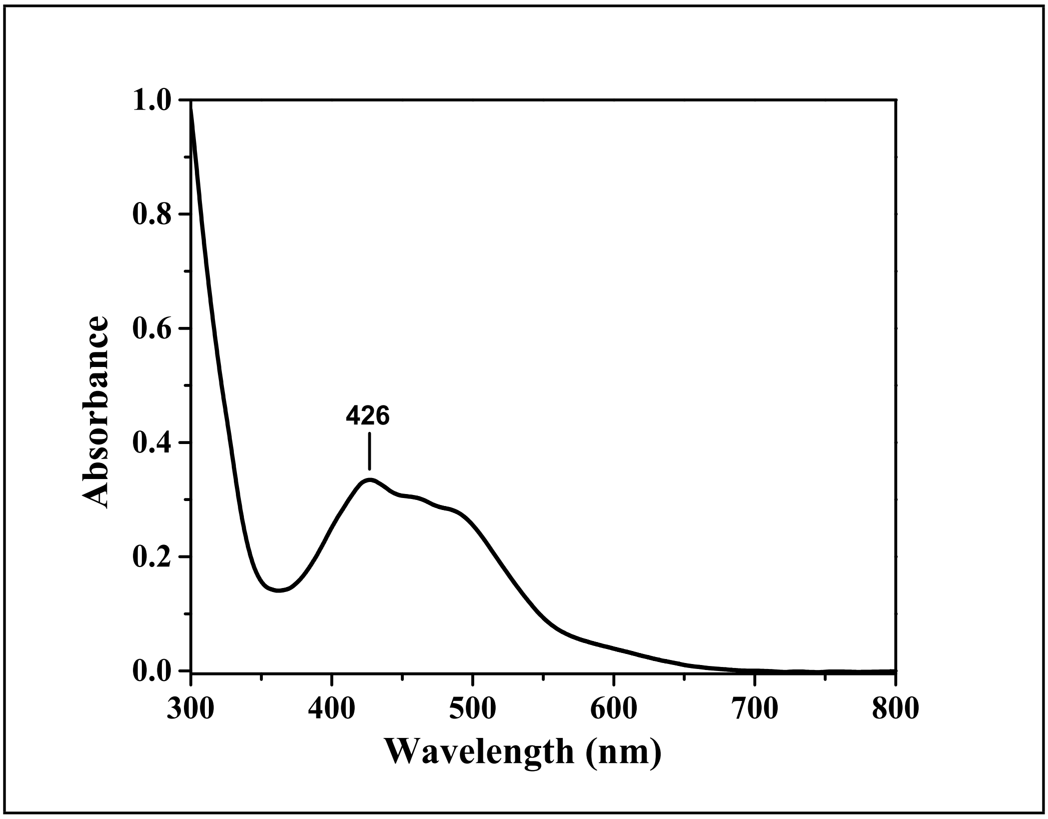

Figure S22: UV-vis spectra of [NiL^{tBu}(SH)] (**3^{tBu}. (Et$_4$N)**) (5x10^{-5}(M) in acetonitrile at 25 °C)

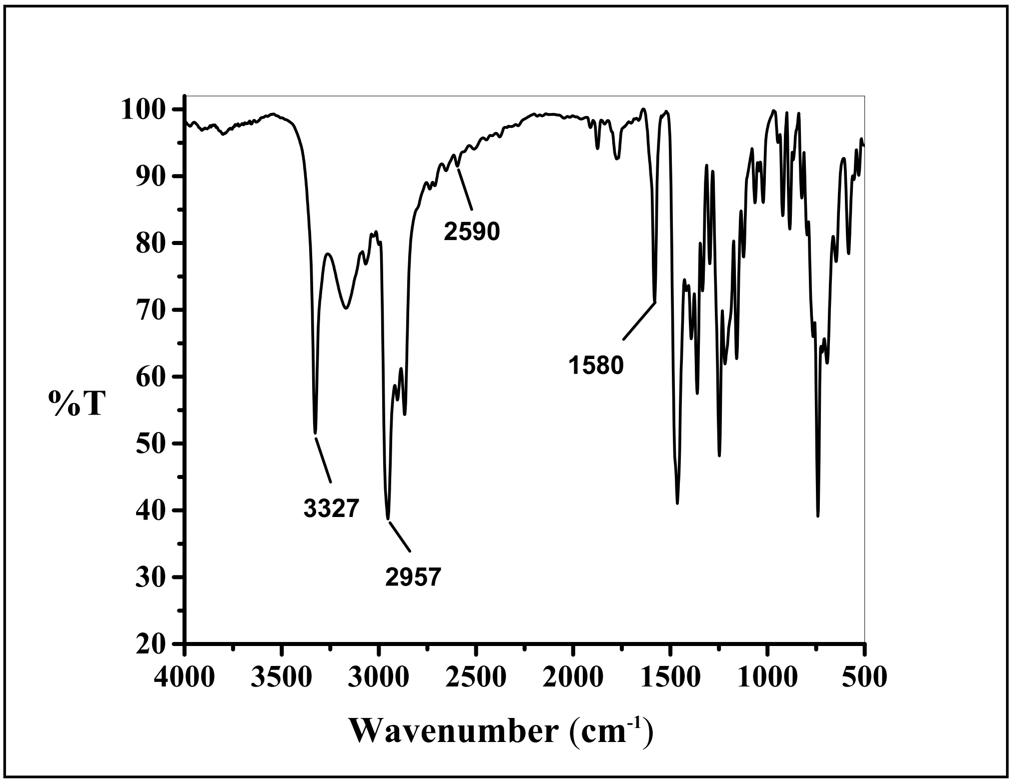

Figure S23: FT-IR (KBr Pellet) spectra of H$_2$L^{tBu}.

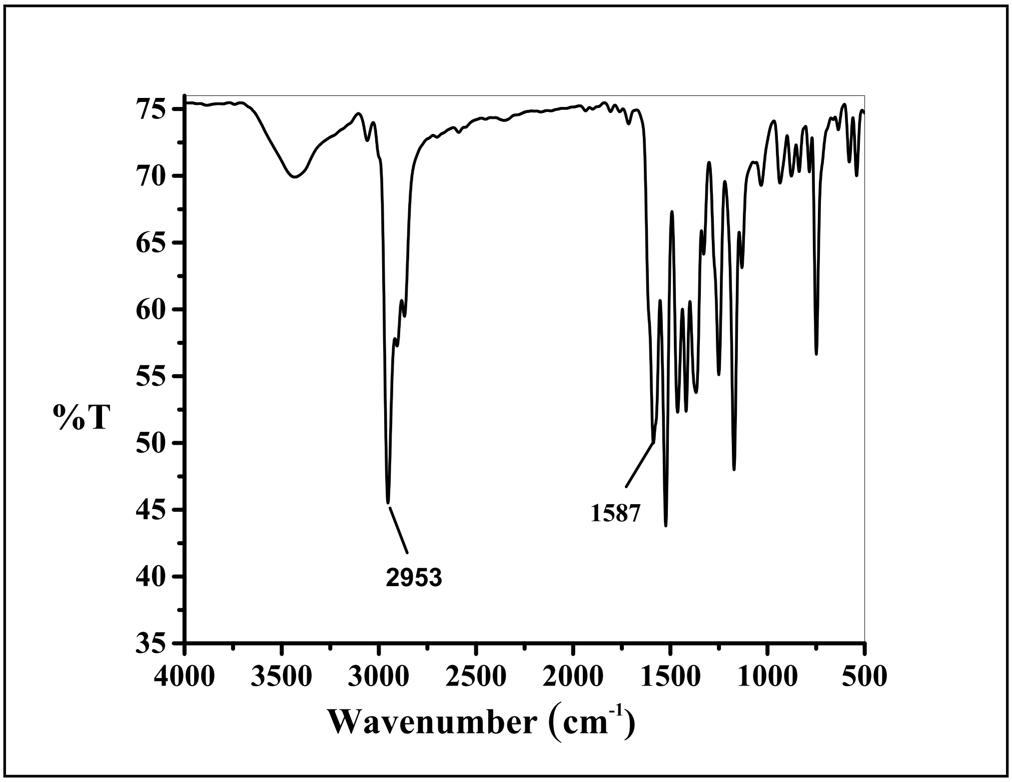

Figure S24: FT-IR (KBr Pellet) spectra of [(NiL^{tBu})$_2$] **(1^{tBu}).**

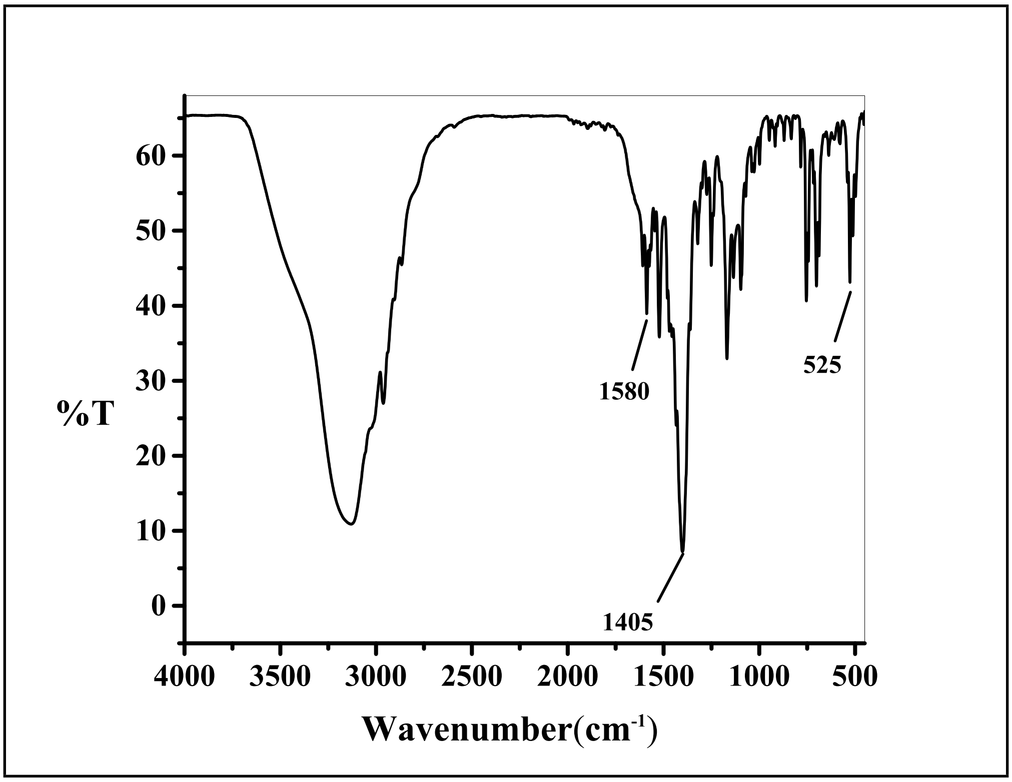

Figure S25: FT-IR (KBr Pellet) spectra of [NiL^{tBu}(PPh$_3$)] (2^{tBu}).

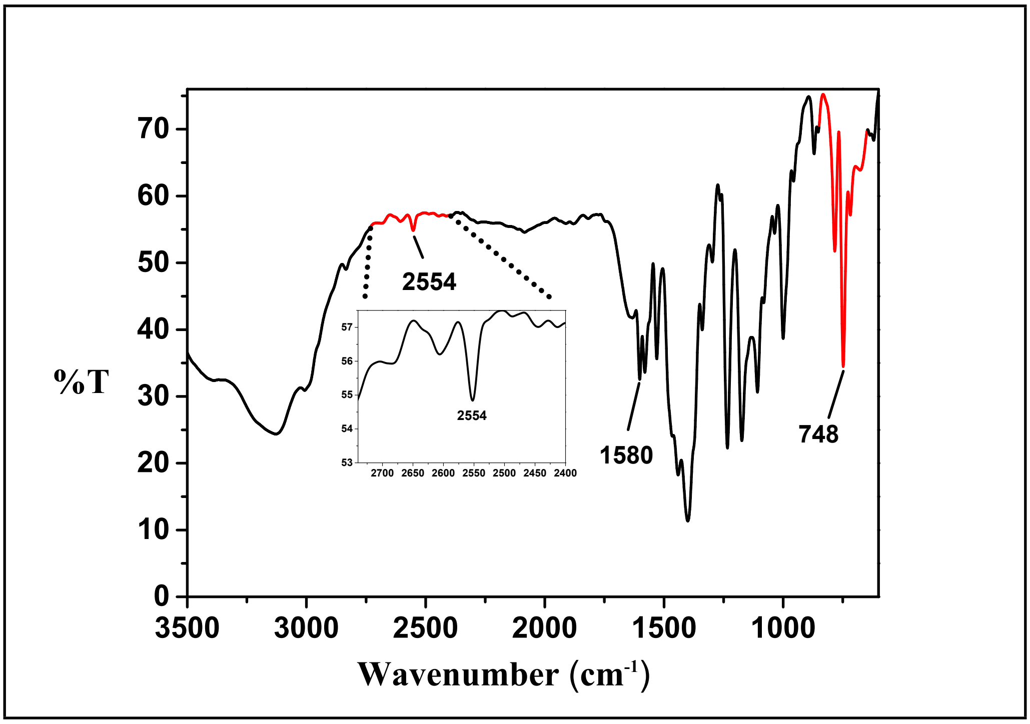

Figure S26: FT-IR (KBr Pellet) spectra of [NiL^{OMe}(SH)] (**3^{OMe}. (Et$_4$N)).**

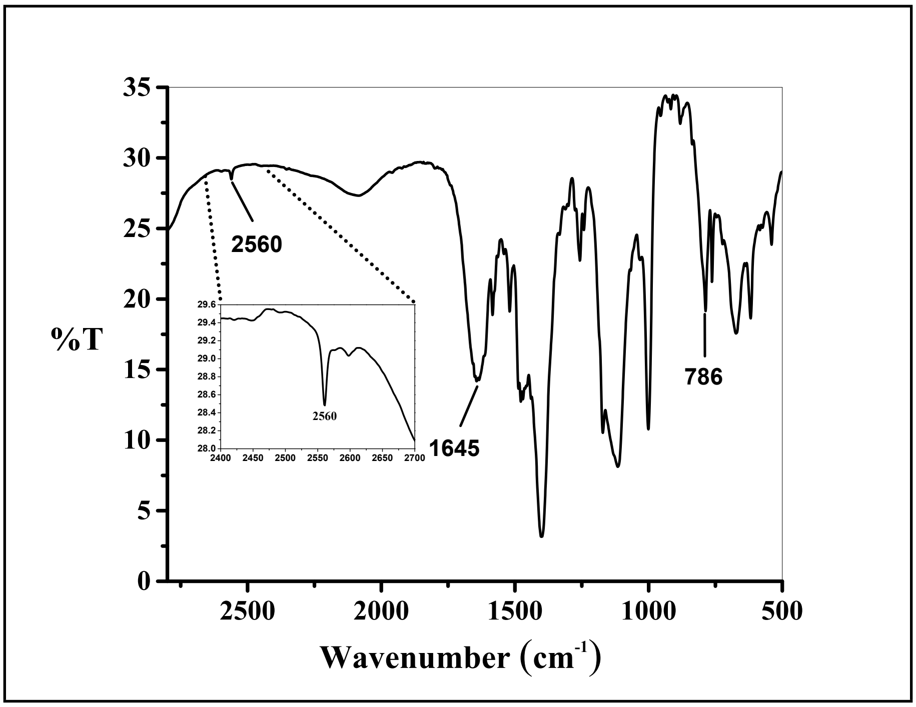

Figure S27: FT-IR (KBr Pellet) spectra of [NiL^{tBu}(SH)] (**3^{tBu}. (Et$_4$N)).**

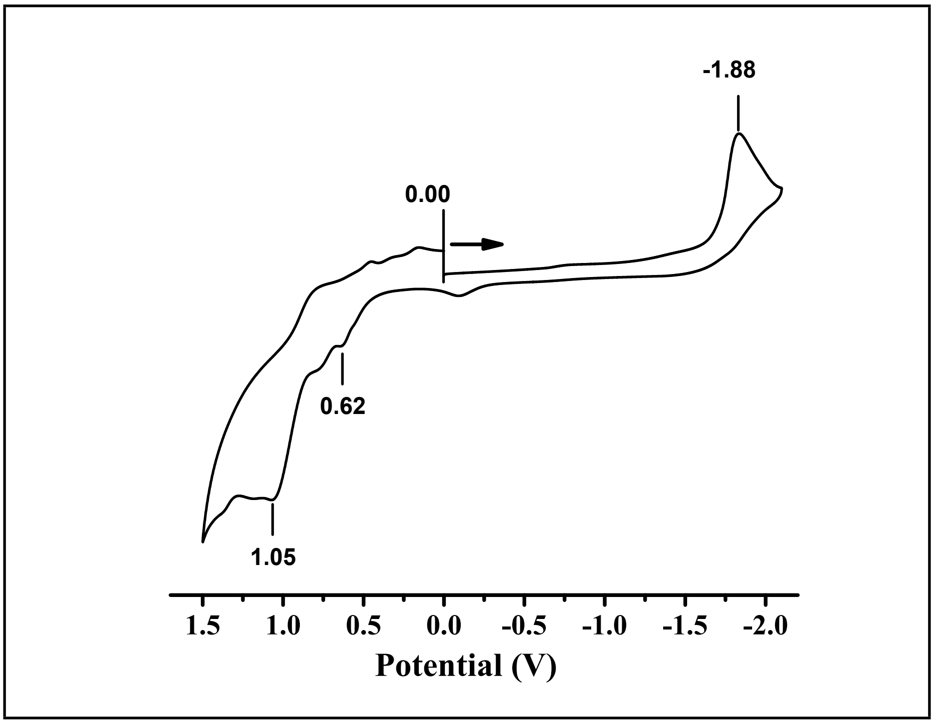

Figure S28: Cyclic voltammogram of H_2L^{OMe} in DMF (scan speed: 100 mV/s, 0.1 M $^{n}Bu_4N(ClO_4)$ supporting electrolyte, glassy carbon working electrode, Pt-wire counter electrode, Ag/AgCl reference electrode, RT, Arrow indicates direction of the scan).

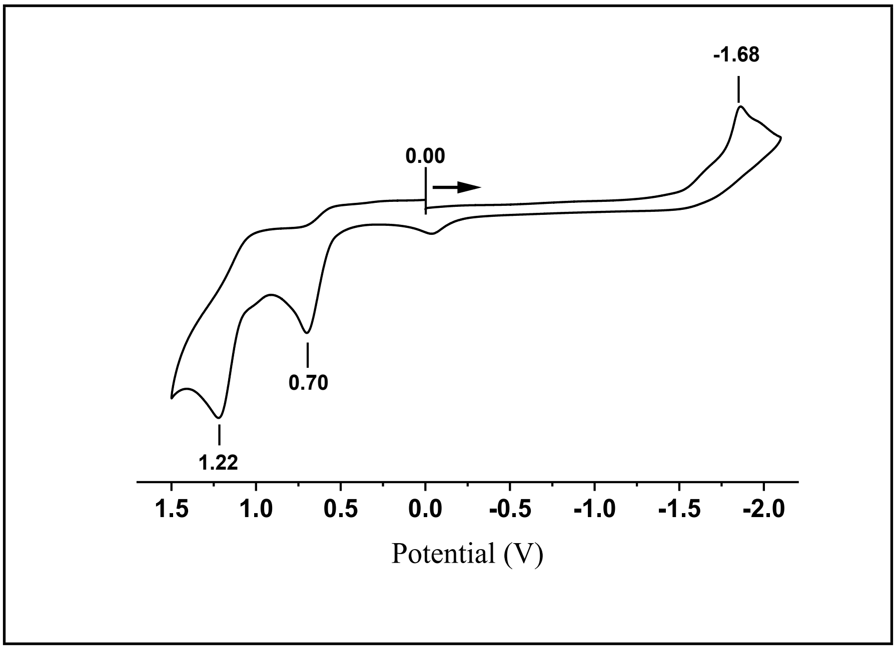

Figure S29: Cyclic voltammogram of H_2L^{tBu} in DMF (scan speed: 100 mV/s, 0.1 M $^{n}Bu_4N(ClO_4)$ supporting electrolyte, glassy carbon working electrode, Pt-wire counter electrode, Ag/AgCl reference electrode, RT, Arrow indicates direction of the scan).

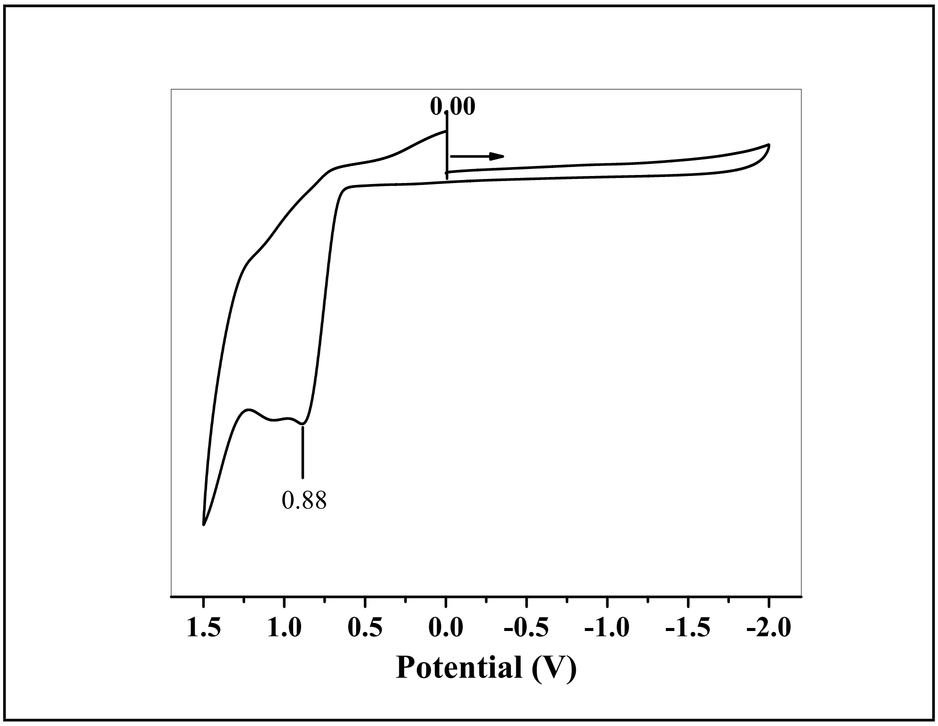

Figure S30: Cyclic voltammogram of NEt_4SH in DMF (scan speed: 100 mV/s, 0.1 M $^{n}Bu_4N(ClO_4)$ supporting electrolyte, glassy carbon working electrode, Pt-wire counter electrode, Ag/AgCl reference electrode, RT, Arrow indicates direction of the scan).

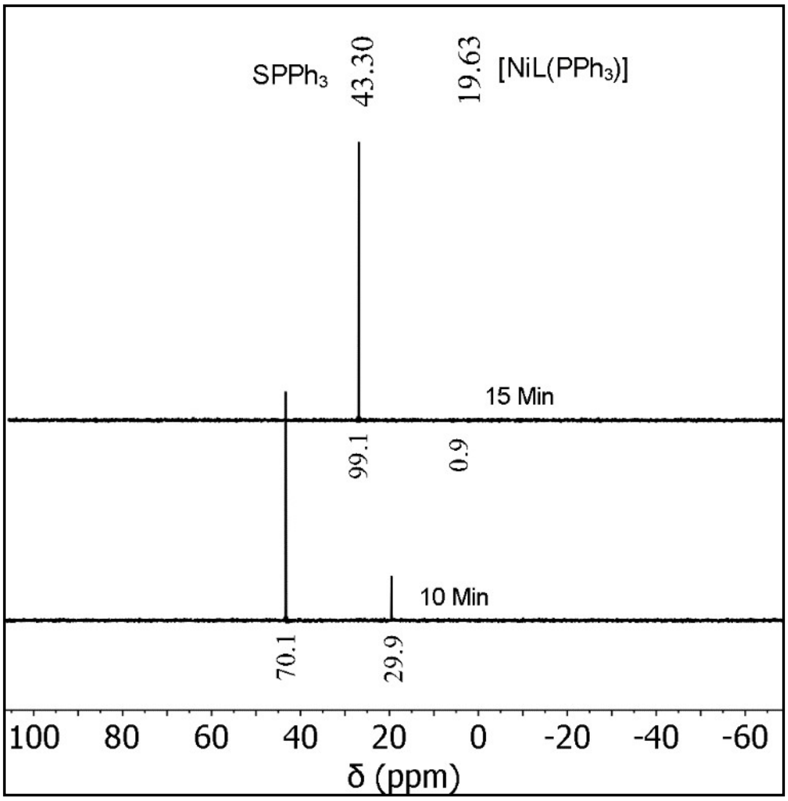

Figure S31: Reaction of $[NiL^{OMe}(PPh_3)]$ with Et_4NSH (1:2.2 ratio) in $CDCl_3$ at 70º C.

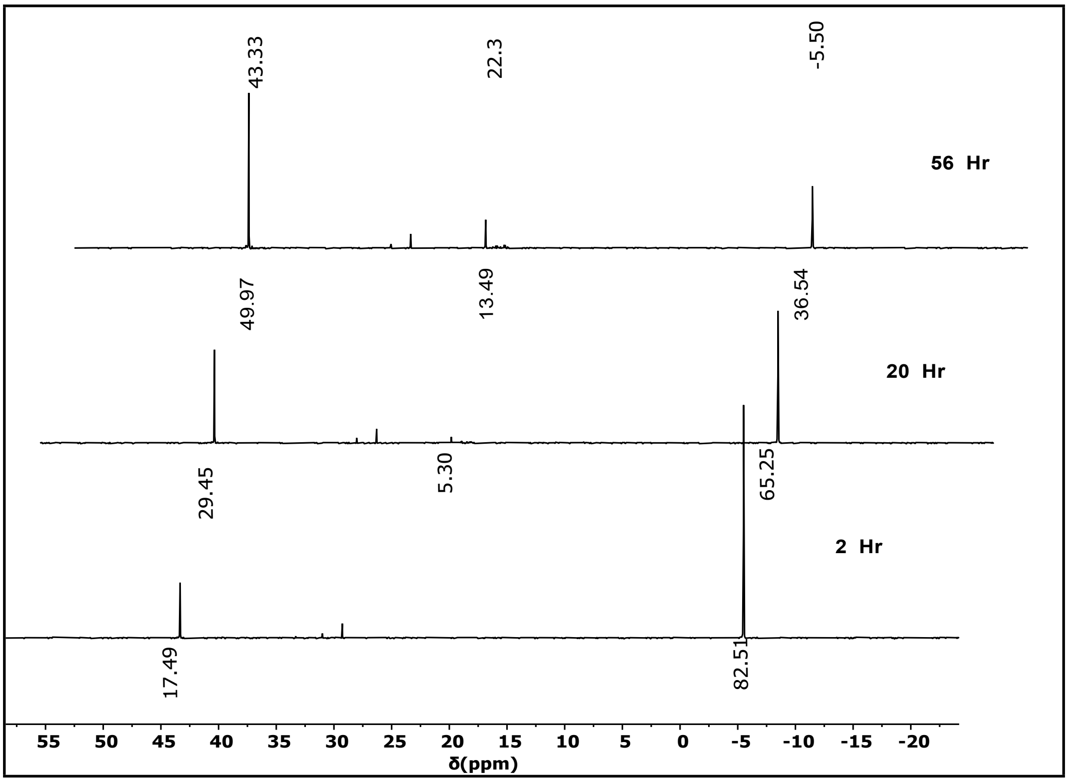

Figure S32. $^{31}P\{^{1}H\}$ NMR spectral changes with time for the reaction of $\mathbf{2^{tBu}}$ and Et_4NSH using 1:1 mol ratio at RT in $CDCl_3$.

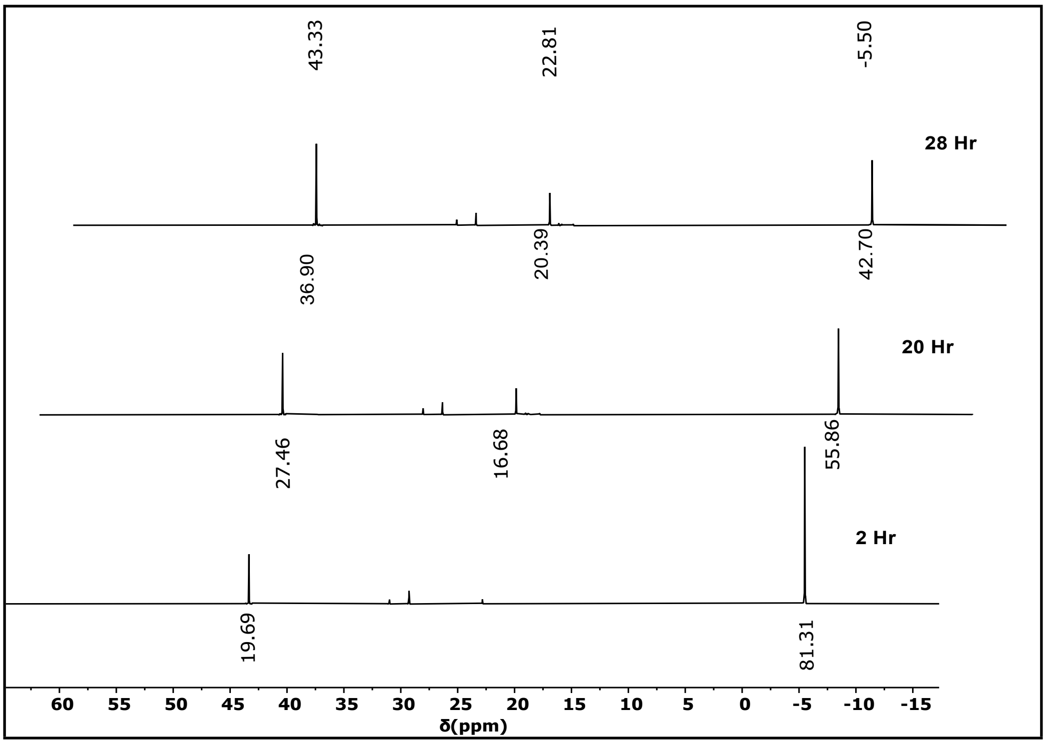

Figure S33. $^{31}P\{^{1}H\}$ NMR spectral changes with time in $CDCl_3$ for the reaction of 2^{tBu} and Et_4NSH using 1:2 mol ratio at RT.

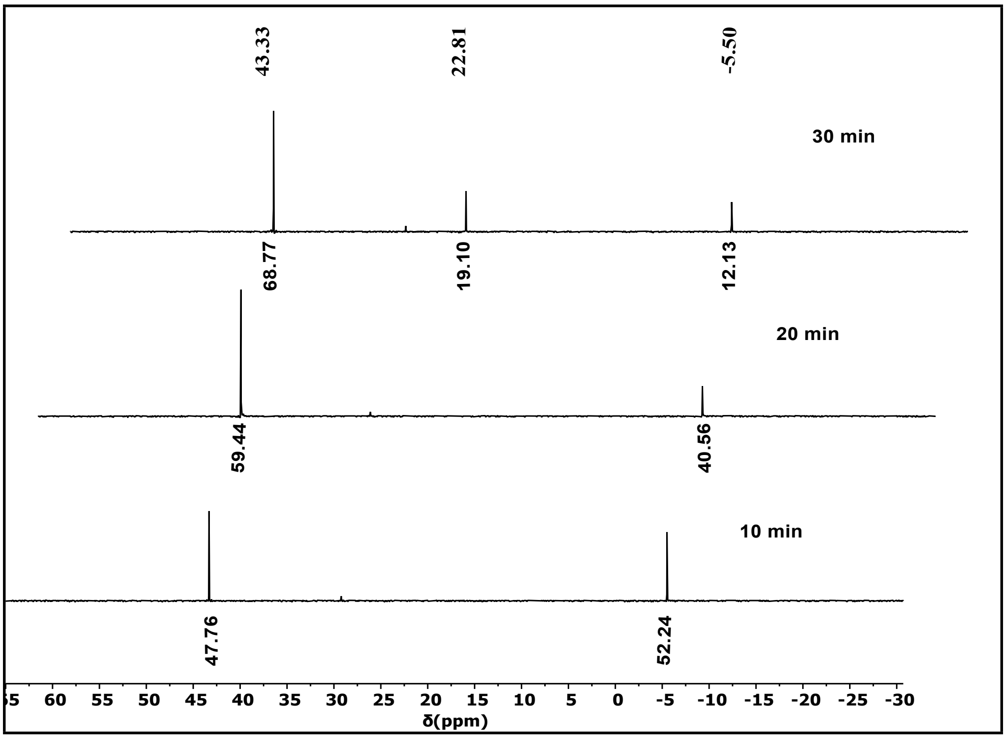

Figure S34: $^{31}P\{^1H\}$ NMR spectral changes with time for the reaction of $\mathbf{2^{tBu}}$ with Et_4NSH (1:2 ratio) in $CDCl_3$ at 70º C.

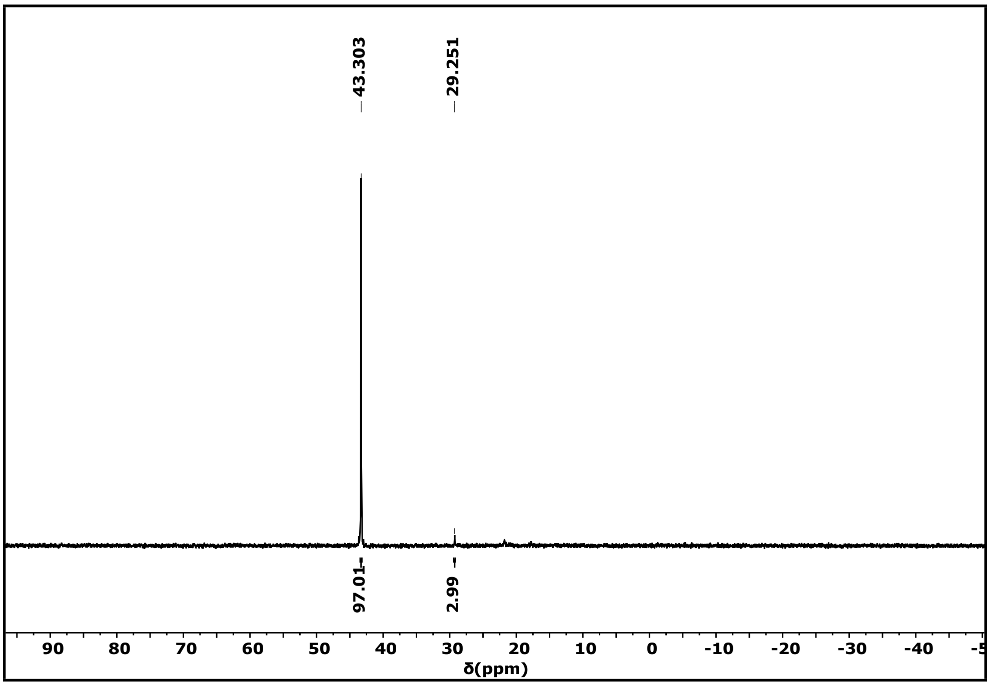

Figure S35. $^{31}P\{^1H\}$ NMR spectral changes with time in $CDCl_3$for the reaction of PPh_3 and Et_4NSH in presence of 10 mol % of complex 2^{tBu} as catalyst at 70 ºC in $CDCl_3$.

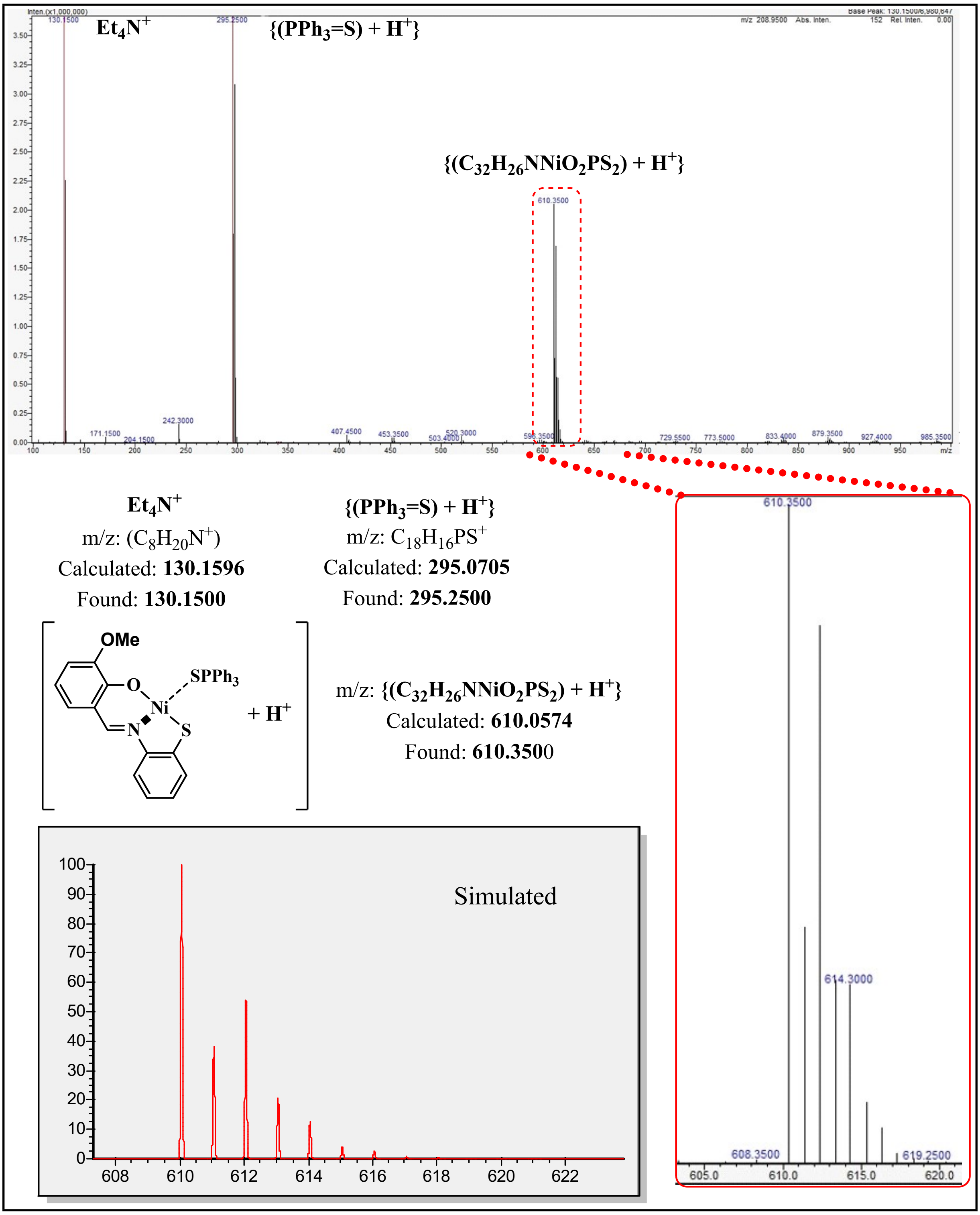

Figure S36: Mass spectra of the reaction mixture of 2^{OMe} with Et$_4$NSH (1:2 ratio) in acetonitrile along with simulated spectrum inset (using Isopro3.0 program).

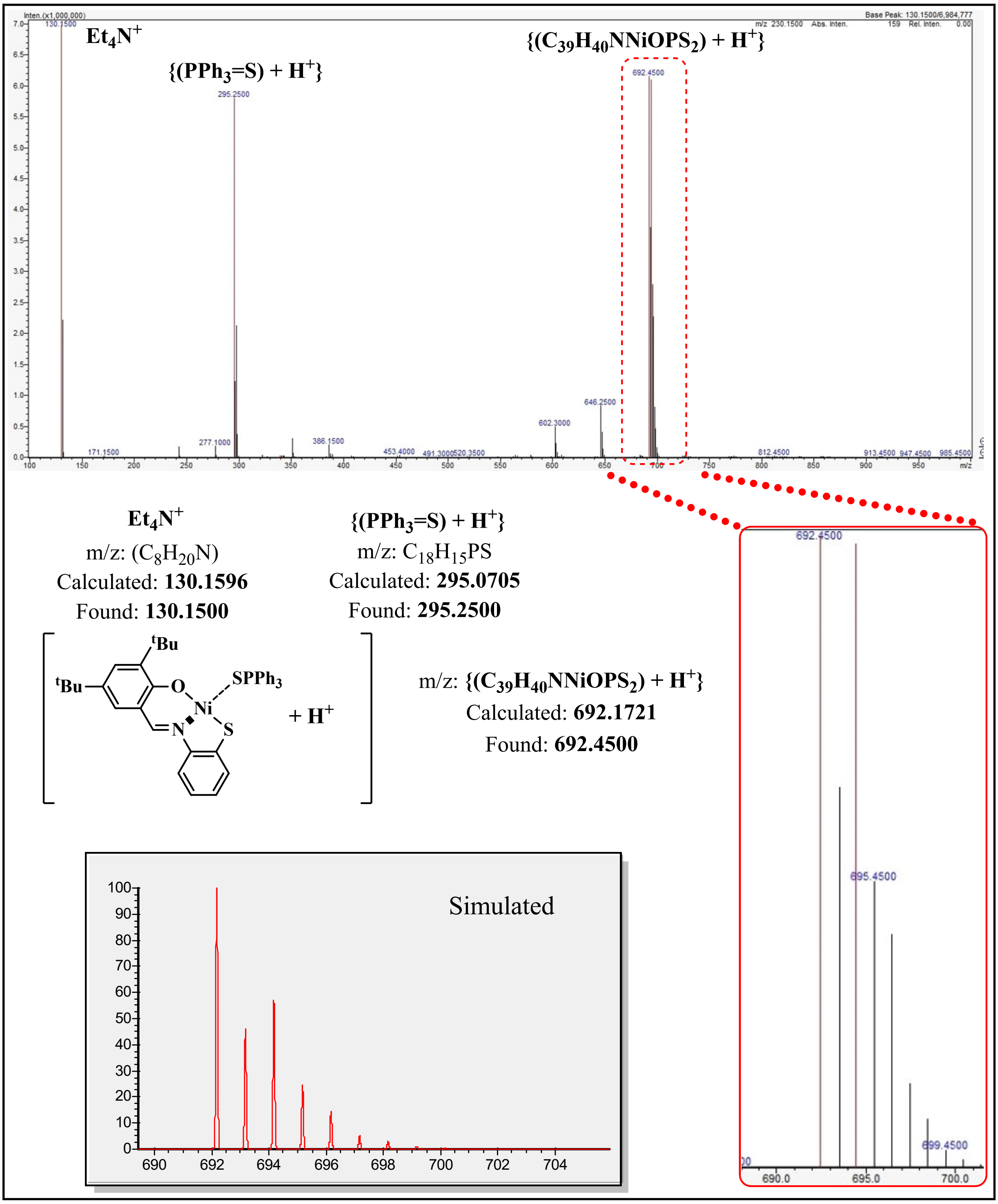

Figure S37: Mass spectra of the reaction mixture of 2^{tBu} with Et_4NSH (1:2 ratio) in acetonitrile along with simulated spectrum inset (using Isopro3.0 program).

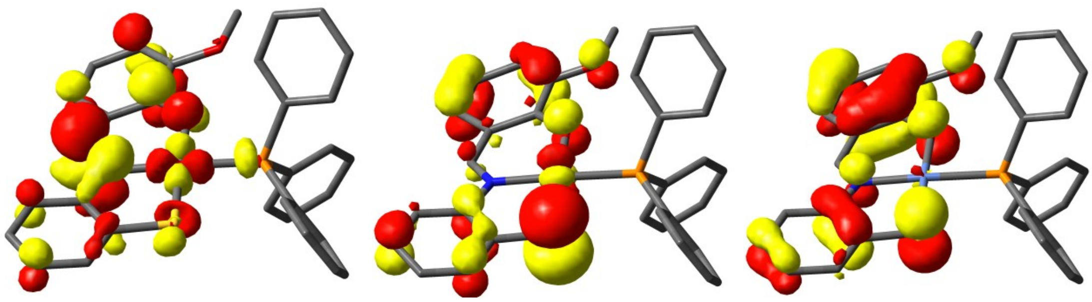

LUMO HOMO HOMO-1

Figure S38: LUMO, HOMO and HOMO-1 of **2**$^{\mathbf{OMe}}$ (geometry optimization using B3LYP/6-311-G+* in DFT methor).

Crystallographic Data Parameters:

Table S1. Crystallographic parameters for Synthesis of $[(NiL^{tBu})_2]$ (**1^{tBu}**), $[NiL^{tBu}(PPh_3)]$ (**2^{tBu}**), $[NiL^{OMe}(SH)]$ (**3^{OMe}. (Et$_4$N)**, $[NiL^{tBu}(SH)]$ (**3^{tBu}.(Et$_4$N)**)

Compound	**1^{tBu}**	**2^{tBu}**	**3^{OMe}. (Et$_4$N)**	**3^{tBu}.(Et$_4$N)**
Identification code	1tBu	2tBu	3OMe	3tBu
Empirical formula	$C_{42}H_{50}N_2Ni_2O_2S_2$	$C_{39}H_{40}NNiOPS$	$C_{22}H_{32}N_2NiO_2S_2$	$C_{29}H_{46}N_2NiOS_2$
Formula weight	796.38	660.46	479.31	561.51
Temperature/K	273.15	101(1)	115.0	100.0(2)
Crystal system	trigonal	orthorhombic	monoclinic	trigonal
Space group	R-3	$Pca2_1$	$P2_1/c$	R3c
a/Å	21.803(6)	19.25730(10)	17.1809(5)	29.6327(3)
b/Å	21.803(6)	13.21440(10)	16.6895(4)	29.6327(3)
c/Å	50.500(10)	13.09390(10)	16.4020(4)	18.1052(2)
α/°	90	90	90	90
β/°	90	90	102.0510(10)	90
γ/°	120	90	90	120
Volume/Å^3	20789(12)	3332.05(4)	4599.5(2)	13768.2(3)
Z	18	4	8	18
ρ_{calc}g/cm^3	1.145	1.317	1.384	1.219
μ/mm^{-1}	0.937	2.115	3.070	2.352
F(000)	7560.0	1392.0	2032.0	5436.0
Crystal size/mm^3	0.25 × 0.18 × 0.12	0.21 × 0.14 × 0.12	0.31 × 0.28 × 0.25	0.25 × 0.2 × 0.12
Radiation	MoKα (λ = 0.71073)	Cu Kα (λ = 1.54184)	CuKα (λ = 1.54178)	Cu Kα (λ = 1.54184)
2Θ range for data collection/°	4.84 to 50.478	6.69 to 136.272	7.466 to 133.362	5.966 to 136.302
Index ranges	-25 ≤ h ≤ 26, -26 ≤ k ≤ 25, -59 ≤ l ≤ 60	-23 ≤ h ≤ 23, -15 ≤ k ≤ 15, -15 ≤ l ≤ 15	-20 ≤ h ≤ 20, -19 ≤ k ≤ 19, -18 ≤ l ≤ 19	-35 ≤ h ≤ 35, -34 ≤ k ≤ 35, -21 ≤ l ≤ 21
Reflections collected	84259	54454	65578	38478
Independent reflections	8307 [R_{int} = 0.0816, R_{sigma} = 0.0377]	5907 [R_{int} = 0.0684, R_{sigma} = 0.0304]	7939 [R_{int} = 0.0902, R_{sigma} = 0.0484]	5518 [R_{int} = 0.0500, R_{sigma} = 0.0309]
Data/restraints/parameters	8307/6/422	5907/1/403	7939/0/598	5518/4/362
Goodness-of-fit on F^2	1.058	1.079	1.091	1.037
Final R indexes [I>=2σ (I)]	R_1 = 0.0857, wR_2 = 0.2122	R_1 = 0.0338, wR_2 = 0.0924	R_1 = 0.0558, wR_2 = 0.1153	R_1 = 0.0410, wR_2 = 0.1093
Final R indexes [all data]	R_1 = 0.1187, wR_2 = 0.2425	R_1 = 0.0344, wR_2 = 0.0933	R_1 = 0.0624, wR_2 = 0.1191	R_1 = 0.0421, wR_2 = 0.1106
Largest diff. peak/hole / e Å^{-3}	1.15/-0.58	0.21/-0.31	0.38/-0.57	0.97/-0.28
Flack parameter	----	-0.035(18)	----	0.37(2)